frontiers | Frontiers in Earth Science

Geochemical, microthermometric, and geochronological characterization of the newly discovered Binnan molybdenum deposit in the great Xing'an Range, northeast China: insights into ore genesis

Zhongyou Qi[1], Shipan Tian[1], Guibin Sun[1], Gang Sun[2]*, Alam Masroor[3], Xiaoyu Li[4] and Bingying Du[1]

[1]Geosciences Research Institute of Heilongjiang, Harbin, Heilongjiang, China, [2]The First Institute of Geological Exploration of Heilongjiang Province, Mudanjiang, Heilongjiang, China, [3]Department of Earth Sciences, Karakoram International University, Gilgit, Pakistan, [4]The Second Institute of Geological Exploration of Heilongjiang Province, Mudanjiang, Heilongjiang, China

In this paper, the Binnan molybdenum (Mo) deposit, a newly discovered deposit located in the Great Xing'an Range, eastern section of the Central Asian Orogenic Belt, has been subjected to a comprehensive integrated study involving field surveys, rhenium-osmium (Re-Os) dating of molybdenite, fluid inclusion analysis, and sulfur-hydrogen-oxygen (S-H-O) isotopic characterization. The mineralization process is divided into three distinct stages: the K-feldspar-quartz stage (I), the quartz-molybdenite stage (II), and the quartz-calcite stage (III). Re-Os isochron dating of molybdenite places the formation of the Binnan Mo deposit during the Late Jurassic, with ages ranging from 142.9 ± 5.1 Ma and 143.7 ± 0.8 Ma. Sulfur isotopic compositions of molybdenite and pyrite, ranging from 1.2‰ to 4.5‰ with a mean of 2.69‰, indicate a magmatic sulfur source of the ore-forming fluids. The hydrogen and oxygen isotopic signatures ($\delta D = -75.5$‰ to -92.3‰; $\delta^{18}O = 13.3$‰-15‰) suggest magmatic fluids that progressively mixed with meteoric water during their evolution. Fluid inclusion study indicates that the mineralization temperatures are ranging from 160°C to 380°C. Integrating these findings with previous studies, we infer that the interplay between fluid mixing and temperature variation was critical in precipitating Mo in the Binnan Mo deposit.

KEYWORDS

Binnan Mo deposit, fluid inclusion, S isotope, Re-Os dating, Great Xing'an Range
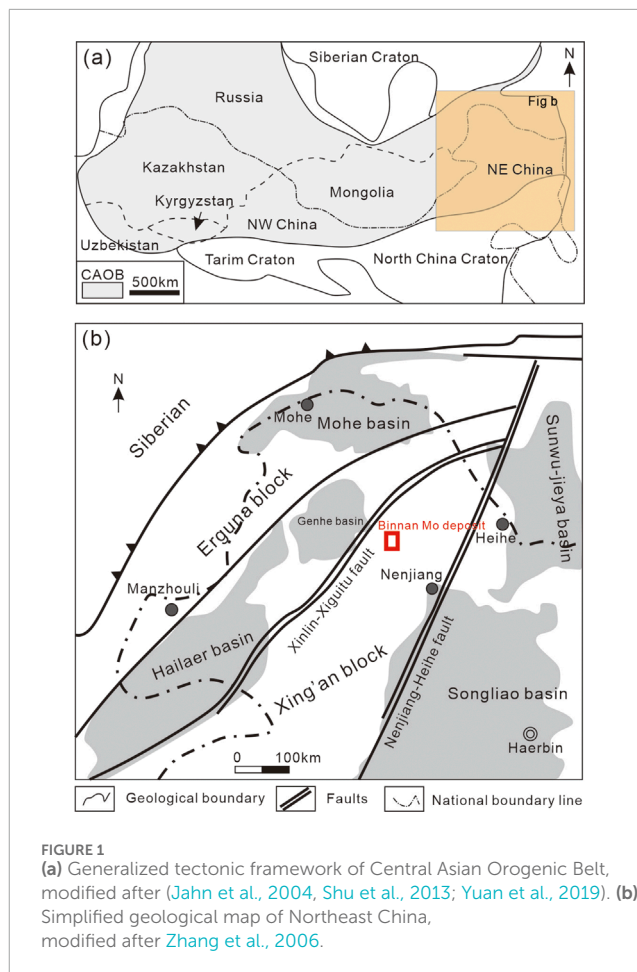
1 Introduction

The Central Asian Orogenic Belt (CAOB), flanked by the Siberian, Tarim, and North China Cratons, is renowned for its diverse metallic mineralization (Zhai et al., 2011; Figure 1A). The Great Xing'an Arc-Basin, situated in the eastern CAOB within northwestern Heilongjiang Province, NE China (Yuan et al., 2018), hosts numerous metal deposits, including the Duobaoshan Cu-Mo, Tongshan Cu-Mo, Zhengguang Au, Yongxin Au, and Erdaokan Ag-Pb-Zn deposits (Liu et al., 2012; Hao et al., 2014; Wang et al., 1997; Yuan et al., 2017; Yuan et al., 2019; Yuan et al., 2023). The Binnan Mo deposit, a newly discovered Mesozoic porphyry Mo deposit, is situated approximately 50 km from the Duobaoshan Cu-Mo deposit (Figure 1).

As a recently discovered deposit, the Binnan Mo deposit has not yet been studied in detail. In this paper, we present an analysis of the ore mineral assemblages, Re-Os geochronology, fluid inclusion petrography, and microthermometry from various ore-forming stages, as well as the S-H-O isotopic compositions of quartz and sulfide from the orebody. These analyses aim to elucidate the source of ore-forming materials, the physicochemical conditions of ore formation, and the mechanism of ore precipitation.

2 Geology of Binnan Mo deposit

2.1 Geological setting

The newly discovered Binnan Mo deposit in Heilongjiang Province is located at the junction of the Great and Lesser Xing'an Ranges (Qi et al., 2017). Its tectonic position is a part of the eastern segment of CAOB, within the Great Xing'an Arc-Basin system. It is adjacent to the Jieya-Bureya Massif of Russia to the east, the Huma Arc-Back Basin to the north, and the Duoboshan Island Arc Belt to the south (Figure 1; Long et al., 2022). The exposed strata comprise the Lower to Middle Ordovician Tongshan Formation of the Paleozoic and the Quaternary of the Cenozoic (Hu et al., 2017). The Lower to Middle Ordovician Tongshan Formation is primarily distributed in the central-northern part of the mining area, trending NWW, with an exposed area of about 0.28 km^2, accounting for 1.22% of the mining area (Qi et al., 2017). This formation has undergone significant metamorphism due to regional dynamic thermal flow, forming a series of intermediate metamorphic rocks. It has also been subsequently affected by dynamic and thermal contact metamorphism. The exposed rocks mainly belong to the upper part of the Tongshan Formation, which is subdivided into upper and lower sections based on lithological characteristics. The lower section consists primarily of biotite-plagioclase-schist and mica-plagioclase schist, while the upper section predominantly comprises biotite-plagioclase gneiss. The Quaternary are exposed in the southwestern part of the mining area, covering approximately 2.97 km^2 or 12.99% of the mining area (Qi et al., 2017). The intrusive rocks are widely exposed in an area of about 19.54 km^2, which constitutes about 85.79% of the mining area. The intrusive rocks are mainly Late Jurassic granodiorite, followed by Late Jurassic monzogranite. Both phases of intrusive rocks in the mining area have been extensively affected by dynamic metamorphism and macroscopically characterized

FIGURE 1
(a) Generalized tectonic framework of Central Asian Orogenic Belt, modified after (Jahn et al., 2004, Shu et al., 2013; Yuan et al., 2019). (b) Simplified geological map of Northeast China, modified after Zhang et al., 2006.
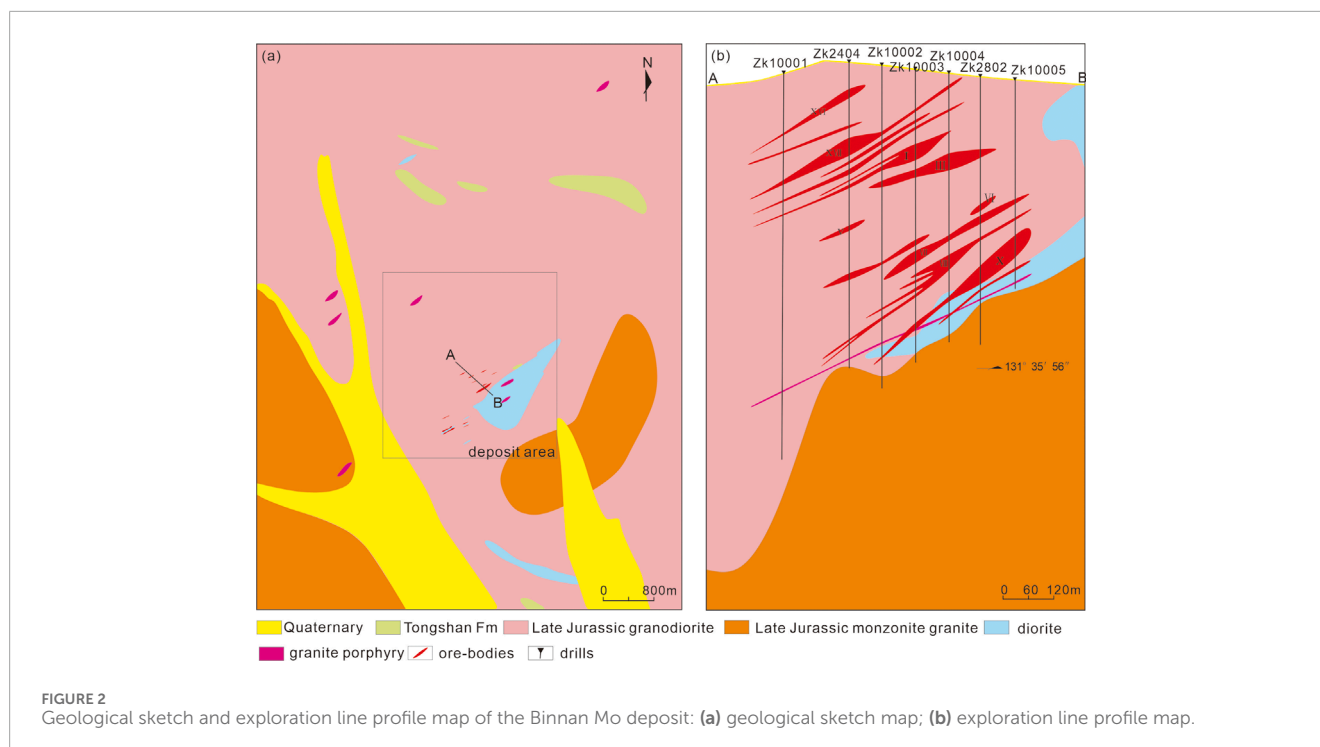
by cataclastic textures. Locally, the rocks have undergone strong hydrothermal alteration displaying features such as potassium feldsparization and alkaline hydrothermal alteration of quartz and plagioclase, forming microcline. The intrusive rocks are closely associated with mineralization, with the granodiorite serving as the host rock for the Binnan Mo deposit.

2.2 Ore characteristics

The Binnan Mo deposit is controlled by a NE-trending fault zone and comprises 38 orebodies that are generally aligned with a northeast orientation (Figure 2A). The orebodies strike 45° NE to NE 50°, and dip towards the NE at an inclination of 18°–34°. Their occurrence is complex, exhibiting irregular lens-shaped, band-like, and layer-like forms, influenced by NE and NW fault structures. The deposit is concealed, can be categorized into three groups of orebodies from shallow to deep. The shallow group is primarily comprised of ore bodies No. I and No. III, the middle group mainly consists of ore bodies No. IV and No. V, and the deep group is dominated by ore bodies No. VII, No. VIII, and No. X, with each group occurring in a coordinated manner (Figure 2B).

The ore-bearing quartz veins are mostly grayish-white and smoky gray, with widths typically ranging from 0.1 to 0.5 m. The extent of the deposit is controlled by hydrothermal alteration zones,

FIGURE 2
Geological sketch and exploration line profile map of the Binnan Mo deposit: **(a)** geological sketch map; **(b)** exploration line profile map.

with the orebodies mainly distributed in the potash feldspathization zone and the silicified-pyritized sericite-quartzite zone. These zones are the centers of alteration and mineralization activities in the Binnan Mo deposit, marking the superimposed areas of multiple episodes of alteration and the concentrated occurrence of Mo ore bodies.

Pyrite is the most abundant metal sulfide in ores, characterized by a pale yellow metallic luster. It primarily occurs in quartz veins, with irregular shapes and a bright yellowish-white color. Pyrite commonly forms anhedral granules, with some crystals well-formed as euhedral to subhedral shapes. Grain sizes range from 0.02 to 3 mm, predominantly between 0.1 and 0.5 mm. It is distributed in disseminated patterns, along veinlet fractures in gangue minerals, and occasionally with molybdenite, chalcopyrite, and other sulfides. Some pyrite is in bay-like contact with gangue minerals or magnetite, even showing mutual inclusion. Magnetite is grayish-brown with a pleochroism of bluish-gray to brownish-yellow, homogeneous to weakly heterogeneous, and exhibits strong magnetism. It occurs as anhedral to subhedral to euhedral granules, with disseminated distribution and irregular crystal shapes. Grain sizes range from 0.02 to 1 mm, with some up to 6.5 mm, mainly between 0.1 and 0.5 mm. Magnetite is mostly found in quartz veins, often associated with pyrite and occasionally with molybdenite. It is also seen in fracture surfaces, forming disseminated veinlets. Fine-grained pyrite can be interlaced with massive magnetite. Chalcopyrite is copper-yellow, weakly heterogeneous, with moderate hardness. It has good polish and is distributed sparsely or along fractures in disseminated veinlets. Some chalcopyrite replaces pyrite and magnetite along edges, while others are replaced by sphalerite along edges or fractures. Chalcopyrite is commonly associated with pyrite and magnetite, occurring in quartz veins with irregular crystal shapes. Grain sizes

generally range from 0.03 to 0.2 mm, with some up to 1.3 mm. Sphalerite is gray with a slight brownish hue, homogeneous, and has moderate hardness. It contains chalcopyrite and forms a droplet-like exsolution with it. It replaces pyrite and chalcopyrite, with grain sizes less than 0.2 mm.

The main gangue minerals include quartz, plagioclase, potassium feldspar, and biotite. Quartz is a major gangue mineral, accounting for about 30% of the ore. It is characterized by shattered, recrystallized interlocking granules, granular serrated interlocking granules, and some elongated granules. It shows wavy extinction and well-developed deformation bands. It replaces feldspar with a replacement sericite structure or in isolated islands. Some form perthitic intergrowth with alkali feldspar. Grain sizes range from 2 to 5 mm. Plagioclase is another major gangue mineral, making up about 30% of the ore. It occurs as subhedral prismatic or tabular grains, with well-developed Carlsbad twinning, pseudo-banded structure, and composition of oligoclase to andesine. It is replaced by alkali feldspar with a sericite structure at the edges.

Based on the paragenetic associations of minerals, the sequence of mineral formation, the textural and structural characteristics of the ores, and the crosscutting relationships of different veins, the ore-forming process is divided into two main stages: the hydrothermal stage and the supergene stage. The hydrothermal stage can be further divided into three ore-forming stages: the K-feldspar-quartz stage (I), the quartz-molybdenite stage (II), and the quartz-calcite stage (III). Mo was primarily precipitated during stage I and II, with stage II being the most significant for Mo mineralization, as it witnessed the highest concentration of various alterations.

During the K-feldspar-quartz stage, mineralization is weak, with minor disseminated molybdenite and pyrite observed in local quartz veins and rock micro-fractures, resulting in sparsely disseminated Mo ore. The main metallic minerals in this stage are magnetite
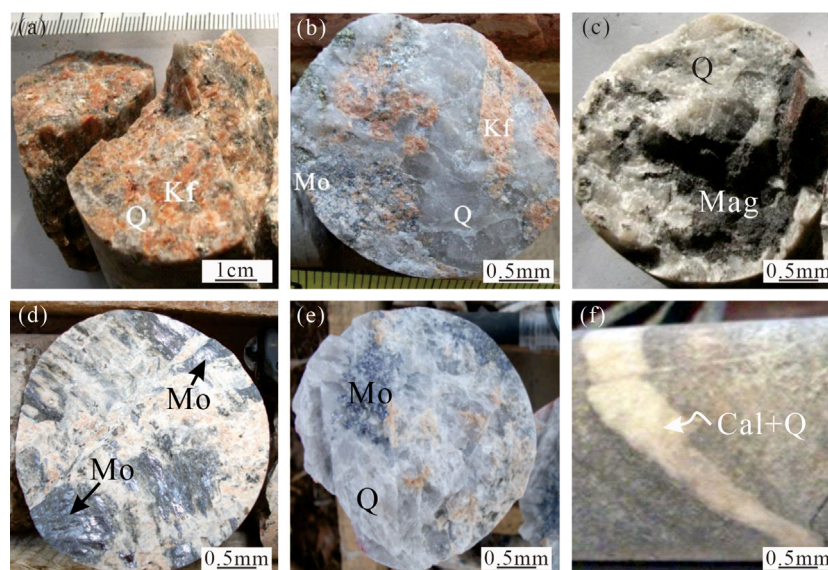
FIGURE 3
Characteristics and crosscutting relationships of ore samples in different ore-forming stages of the Binnan Mo deposit; **(a)** potash feldspathization ore; **(b)** molybdenite-bearing, potash feldspathization quartz vein in K-feldspar-quartz stage; **(c)** quartz-magnetite veins in K-feldspar-quartz stage; **(d)** molybdenite in quartz-molybdenite stage; **(e)** quartz-molybdenite veins; **(f)** quartz-calcite vein in late stage; Q, Quartz; Py, Pyrite; Mo, Molybdenite; Mag, Magnetite; Kf, K-feldspar; Cal, Calcite.

and pyrite, with gangue minerals primarily consisting of quartz, plagioclase, K-feldspar, and biotite (Figures 3A, B). Molybdenite is mostly idiomorphic. Pyrite is mostly idiomorphic to subhedral, and magnetite is mostly subhedral to xenomorphic.

The quartz-molybdenite stage is the main ore-forming stage, characterized by large-scale silicification, K-feldspathization, and sericitization. This stage produced various molybdenite-bearing quartz veins, including quartz-pyrite-molybdenite veins, and quartz-K-feldspar-molybdenite veins (Figures 3C–E). Significant molybdenite production occurred in this stage with molybdenite appearing as scattered disseminations or irregular aggregate masses within or along the edges of quartz veins (Figure 4). Some molybdenite formed as flaky or curved leaf-like aggregates, filling the veins along the micro-fractures of the gangue minerals.

The quartz-calcite stage represents a low-temperature hydrothermal phase, primarily forming quartz-calcite veins, quartz-calcite-fluorite veins, or chlorite veins (Figure 3F). These are more widely distributed and often occur in later-stage structural fractures, cutting across the veins from the earlier stages. Minor fine-grained pyrite was locally produced, but Mo mineralization during this stage was weak or negligible, marking the late stage of ore formation.

3 Sampling and methodology

3.1 Sampling

Over 50 samples, collected from various drill cores (ZK10003, ZK10004, ZK10005, ZK10402, ZK10404, ZK10303, etc.), were subjected to petrographic study. Of these, 30 samples, representing all three mineralization stages, were prepared as polished thin sections for microscopic examination. Among these, nine thin sections—three each from the K-feldspar-quartz stage, quartz-molybdenite stage, and quartz-calcite stage—were prepared for fluid inclusion analysis. Additionally, five samples from drill cores ZK10003, ZK10004, ZK10005, ZK100402, and ZK100404, were selected for hydrogen and oxygen isotopic analysis. Eight samples of pyrite and molybdenite extracted from the orebodies were selected for sulfur isotope analysis. Furthermore, seven samples of molybdenite from drill cores ZK10402, ZK10303, ZK10004, ZK10003, ZK10404, ZK2404, and ZK10405 were designated for Re-Os isotopic analysis.

3.2 Methodology

Microthermometric analysis was performed using a Linkam THMSG 600 heating-freezing stage, integrated with a ZEISS microscope at the China University of Geosciences, Wuhan. The temperature range was set to standard values from −60°C to 400°C. The estimated precision for freezing and heating measurements was ±0.1°C (from −60°C to 25°C), ±1°C (from 25°C to 300°C), and ±2°C (above 300°C).

H-O isotope analyses were performed at the Beijing Research Institute of Uranium Geology (BRIUG), employing a Delta V advantage stable isotope ratio mass spectrometer coupled with a TM-SPCL MIR10 infrared laser. The accuracy for oxygen isotope analysis was better than ±0.2‰, while for hydrogen isotope analysis, it was better than ±2‰. The isotopic ratios are reported in the standard δ notation (‰) relative to SMOW.

The pyrite grains were carefully separated using a binocular microscope and cleaned using an ultrasonic cleaner to remove any adhering impurities. The grains were then ground to a 200-mesh fineness with an agate mortar to ensure sample homogeneity
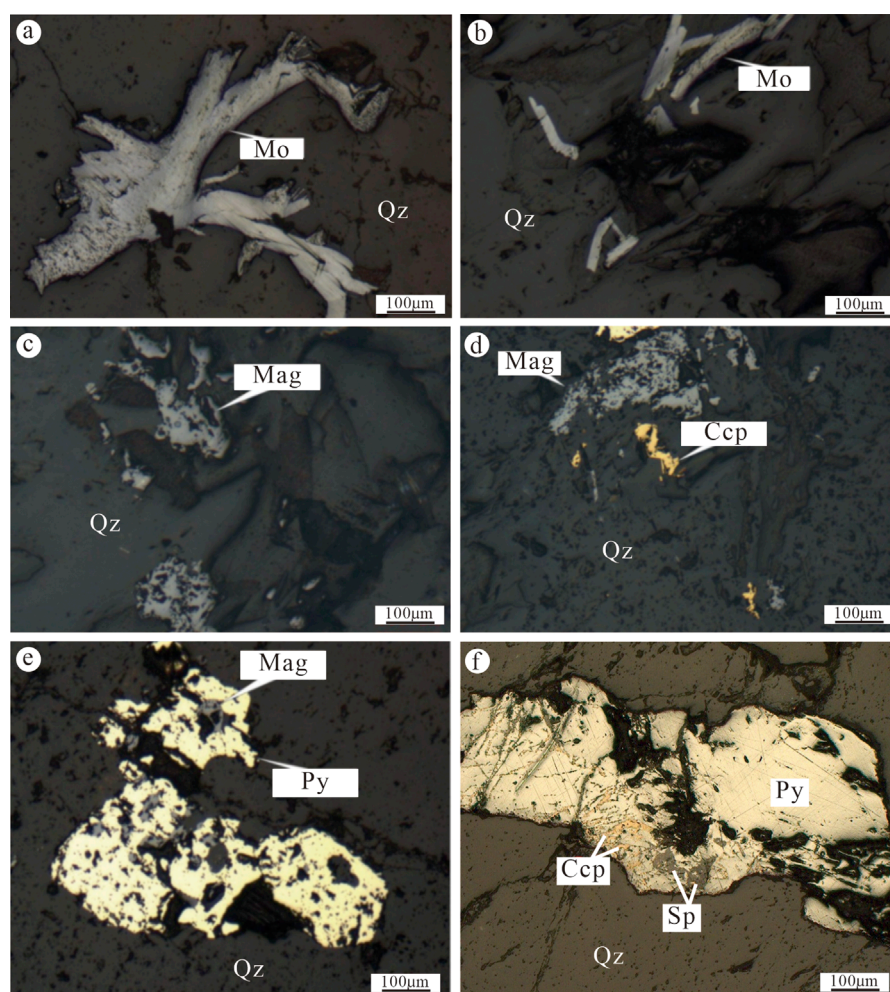
FIGURE 4
Features of minerals under microscope. **(a)** dendritic molybdenite (Mo) in quartz (Qz) veins; **(b)** girdle molybdenite in quartz veins; **(c)** disseminated magnetite (Mag), irregular crystalline form; **(d)** chalcopyrite (Ccp) disseminated in quartz veins, irregular crystalline form; **(e)** disseminated vented pyrite (Py) coated with fine-grained magnetite; **(f)** chalcopyrite and sphalerite (Sp) coated within pyrite.

for isotopic analysis. The S isotope analysis was conducted at the Beijing Research Institute of Uranium Geology using a Delta V plus r stable isotope mass spectrometer following the procedures outlined by Glesemann et al. (1994). The results are expressed in $\delta^{34}S$-VCDT with an analytical precision of ±0.2‰, relative to the Vienna Canon Diablo Troilite (VCDT) sulfide standard with $\delta^{34}S$ = 0.0‰ by definition.
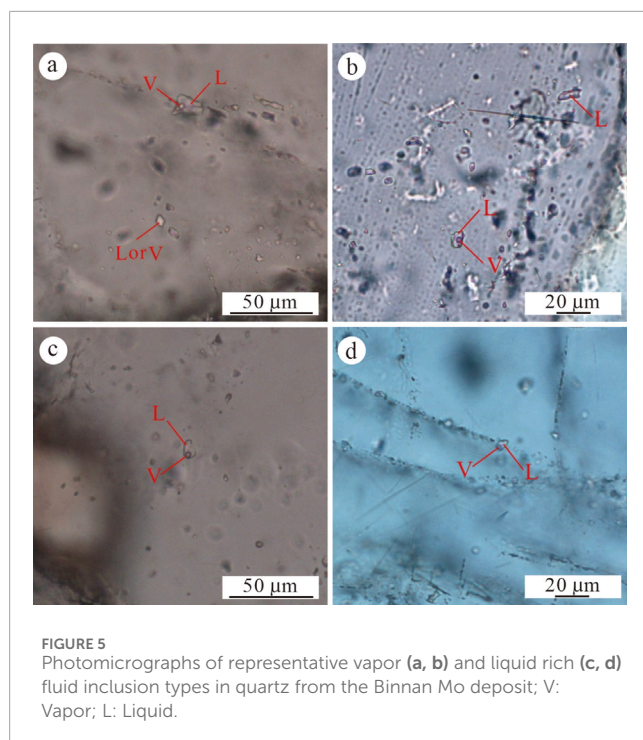
4 Results

4.1 Occurrence of Mo

Molybdenite in the deposit is predominantly found within quartz veinlets and fracture surfaces, with a smaller portion occurring within quartz monzonite dikes. Molybdenite are primarily classified into two distinct categories. First category is characterized by bright white, lamellar or scaly aggregates occurring within quartz veins (Figure 4), predominantly euhedral to subhedral

in habit, with scaly molybdenite particles less than 0.04 mm in size, which are challenging to discern individually. In contrast the lamellar molybdenite particles are coarser, ranging from 0.1 to 1 mm in size, and occasionally display a banded pattern. The second category of molybdenite appears as bright silver-gray scaly, disseminated or veinlet-disseminated within and adjacent to mineralized micro-quartz veins. It fills fractures in the gangue minerals in vein-like or disseminated vein patterns. This type is often associated with pyrite and magnetite, and exhibits a heterogeneous distribution. The particle sizes in this category generally range from 0.04 to 0.5 mm (Figure 4).

4.2 Fluid inclusion study

The fluid inclusions within the quartz veins of the Binan Mo deposit are relatively small and sparse, primarily consisting of primary, secondary, and pseudo-secondary inclusions. Based on the morphology of the inclusions, the primary inclusions can be further

FIGURE 5
Photomicrographs of representative vapor **(a, b)** and liquid rich **(c, d)** fluid inclusion types in quartz from the Binnan Mo deposit; V: Vapor; L: Liquid.

classified into liquid-gas inclusions and liquid-only inclusions, with the liquid-gas inclusions predominantly being liquid-rich (Figure 5).

The liquid-only inclusions are predominantly rectangular, elliptical or irregular in shape, with sizes ranging from 1 to 5 μm. These inclusions are mostly randomly distributed within the quartz veins and quartz phenocrysts, accounting for approximately 10% of the total inclusion population. However, most of these liquid fluid inclusions probably are not primary.

The liquid-rich inclusions are primarily rectangular, elliptical or irregular in shape, with gas fill percentages ranging from 5% to 50%, and most commonly between 10% and 25%. Their sizes typically range from 2 to 5 μm, with the majority falling within the 2–3 μm range. Most of these inclusions are randomly distributed within the quartz veins and quartz phenocrysts, a minority exhibits preferential alignment along the growth direction of the quartz grains. These inclusions are well developed and account for approximately 70% of the total inclusion population.

4.3 Microthermometry

Microthermometric measurements of fluid inclusions in quartz were conducted following the sequence of freezing before homogenization. Among all types of inclusions, liquid-rich inclusions are numerically dominant; thus, the homogenization temperatures were primarily determined using these liquid-rich inclusions as the subject of analysis.

A total of 103 homogenization temperatures of quartz from three ore-forming stages were tested, and a histogram was plotted (Figure 6). The overall range of homogenization temperatures is between 133.3°C and 421.3°C, with three distinct peaks occurring at 360°C–380°C of K-feldspar-quartz stage,

250°C–260°C of quartz-molybdenite stage, and 160°C–180°C of quartz-calcite stage, respectively. These peaks correspond to the previously identified mineralization stages. During the mineralization process of the Binan Mo deposit, quartz is commonly present, aligning with the three peaks observed in the homogenization temperature tests. The temperature range for the main mineralization stage is 250°C–380°C.

4.4 Hydrogen-oxygen-sulfur isotopes

Eight samples containing molybdenite and pyrite were uniformly collected from the hydrothermal potassic-feldspathized granodiorite (host rock) and the mineralized quartz veins in the central part of the ore field for sulfur isotope analysis. These included three samples of molybdenite and five samples of pyrite. The results show that molybdenite and pyrite from different mineral assemblages exhibit a relatively uniform sulfur isotopic composition, with $\delta^{34}S$ values ranging from 1.2‰ to 4.5‰, predominantly stable around 3‰, with an average value of 2.69‰ (Table 1).

The hydrogen and oxygen isotope compositions of five quartz samples from molybdenite-bearing quartz vein yield δD values relative to SMOW ranging from −75.5‰ to −92.3‰ and $\delta^{18}O$ values from 13.3‰ to 15‰ (Table 1). Calculations based on these values result in $\delta^{18}O_{water}$ values ranging from 6.3‰ to 8‰. On the δD-$\delta^{18}O_{water}$ diagram, the projection points of hydrogen and oxygen isotope compositions of ore from the deposit are located to the lower right of the primary magmatic water, and within the realm of meteoric water (Figure 7).
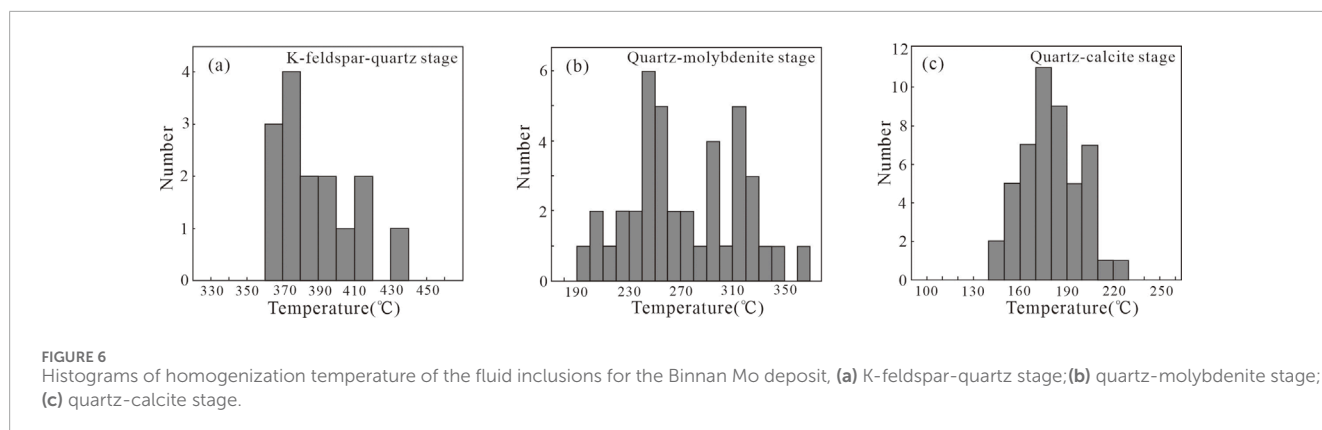
4.5 Re-Os isotopes

In this study, seven molybdenite samples were selected for Re-Os dating analysis. Six of these samples showed ^{187}Re and ^{187}Os concentrations ranging from 32.58 to 47.42 ppm and 78.28–113.6 ppb, respectively. The model ages of the seven samples varied between 143.4 ± 2.1 Ma and 144.0 ± 2.0 Ma, with a weighted mean age of 143.7 ± 0.8 Ma. Isoplot software calculations yielded an isochron age of 142.9 ± 5.1 Ma with an MSWD of 0.055. The consistency between the weighted mean age and the isochron age indicates that the Re-Os system remained closed. The calculated age of 142.9 ± 5.1 Ma to 143.7 ± 0.8 Ma represents the mineralization age of the Binnan Mo deposit, which formed during the Late Jurassic to Early Cretaceous (Table 2; Figure 8).

5 Discussions

5.1 Source of ore-forming fluid

The sulfur isotopic composition provides insights into physical and chemical conditions of sulfide formation and the sources of metallogenic materials. The $\delta^{34}S$ values of molybdenite and pyrite from the Binnan Mo deposit range from 1.2‰ to 4.5‰ with an average of 2.69‰ (Table 1; Figure 9), indicating a uniformity in the ore-forming fluids, which suggests a magmatic source ($\delta^{34}S = 0‰ ± 5‰$; Ohmoto and Rye, 1979). These $\delta^{34}S$ values are comparable

FIGURE 6
Histograms of homogenization temperature of the fluid inclusions for the Binnan Mo deposit, **(a)** K-feldspar-quartz stage;**(b)** quartz-molybdenite stage; **(c)** quartz-calcite stage.

TABLE 1 H-O-S isotopic compositions of quartz (Qz), molybdenite (Mot) and pyrite (Py) from the Binnan Mo deposit.

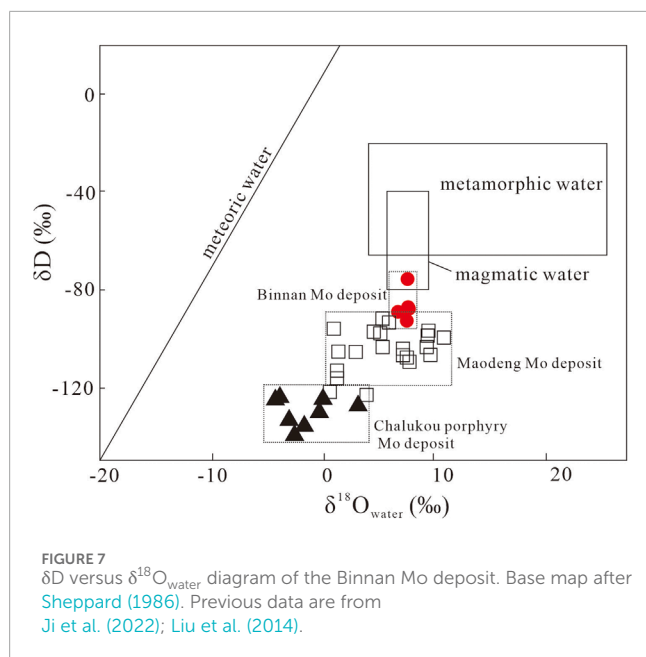| Sample no.	Sample Property	Mineral	δD_{SMOW} (‰)	$\delta^{18}O_{SMOW}$ (‰)	$\delta^{34}S_{V-CDT}$ (‰)
ZK10003T2	Molybdenite-bearing quartz vein	Qz	−75.5	14.1	—
ZK10004T1			−88.7	13.3	—
ZK10005T1			−92.3	14.8	—
ZK10402T1			−87.7	15.0	—
ZK10404T1			−87.3	14.9	—
ZK10003T1	Granodiorite	Py	—	—	3.3
ZK10005T1			—	—	1.2
ZK10404T1			—	—	3.1
ZK10004T1	Molybdenite-bearing quartz vein	Mot	—	—	3.2
ZK10402T1		Mot	—	—	4.5
ZK10005T1		Mot	—	—	2.1
ZK10402T1		Py	—	—	2.8
ZK10004T2		Py	—	—	1.3

to those of the Aolunhua porphyry Cu-Mo deposit (1.6‰–4.9‰, Ma and Chen, 2011), the Maodeng porphyry Mo deposit (−6.0‰ to −0.49‰, Ji et al., 2022), the Bairendaba Ag-Pb-Zn deposit (−4.0‰–1.6‰, Chen et al., 2018) and the Dajing Sn-Cu-Pb-Zn deposit (−1.8‰–3.8‰, Chu et al., 2002), likely due to degassing of parent magma (Zheng et al., 1996).

The H-O isotopic compositions of ore minerals can reveal the nature and genesis of mineralized fluid. In Binnan Mo deposit, the $\delta^{18}O_{water}$ and δD values of 13.3‰–15‰ and −75.5‰ to −92.3‰, respectively, are lower than those of primary magmatic water ($\delta^{18}O_{water}$ = 5.5‰–9.5‰ and δD = −80‰ to −40‰; Sheppard, 1986). The characteristics of H-O isotopic compositions of quartz from Binnan Mo deposit align with those of porphyry Mo deposits, such as Chalukou and Maodeng (Ji et al., 2022; Liu et al., 2014). In the $\delta^{18}O_{water}$ versus δD diagram (Figure 7), the

samples plot between magmatic and meteoric water lines, closer to magmatic region, indicating that the ore forming fluids were primarily derived from deep intrusions, with limited dilution by meteoric water.
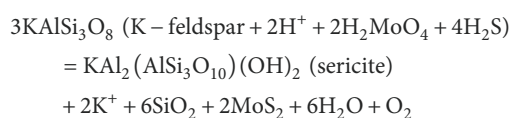
5.2 Mineralization age

The mineralization is linked to the magmatic activity, as evidenced by zircon U-Pb dating which reveals a close spatial relationship between the Binnan Mo deposit and the associated granite pluton (Qi et al., 2017). The preciously reported zircon U-Pb age of the granitic pluton is 155.5 ± 1.5 Ma, consistent with large-scale Mo mineralization in Northeast China (Du et al., 2010). Re-Os isochron age of molybdenite samples yields ages of 142.9 ± 5.1 Ma to 143.7 ± 0.8 Ma, providing a reliable constraint on

FIGURE 7
δD versus $\delta^{18}O_{water}$ diagram of the Binnan Mo deposit. Base map after
Sheppard (1986). Previous data are from
Ji et al. (2022); Liu et al. (2014).

the timing of Mo mineralization. Since the Early Mesozoic, the Great Xing'an Range has been influenced by the subduction of the Mongol-Okhotsk plate resulting in the formation of numerous NE-NNE and NW-trending fault structures, such as the Derbugan fault. These tectonic features facilitated intense magmatic and volcanic activities, producing widespread medium-to-acid intrusive and volcanic rocks and triggering large-scale metallogenic events. Mo mineralization in the Greater Xing'an Range primarily occurred during the middle to late Mesozoic and was closely related to magmatic activity related to the subduction collision of the northern Mongol-Okhotsk Ocean (Shu et al., 2016).

5.3 Mo precipitation mechanism

Experimental studies have demonstrated that Mo is predominantly transported as $HMoO_4^-$ and H_2MoO_4 in solutions of low to medium salinities (<11 wt% NaCl equivalent) (Kudrin, 1989; Ulrich and Mavrogenes, 2008). At higher salinities (>20 wt% NaCl equivalent), molybdenum-oxygen-chloride complexes become significant. Temperature, pH, and redox potential [lgf (O_2)] variations of metallogenic fluids influence Mo precipitation (Cox et al., 2001; Shu et al., 2019). The ore-forming fluids at the Banin Mo deposit exhibit a broad temperature range (133.3°C–421.3°C), supporting the transport of molybdenum as $HMoO_4^-$, H_2MoO_4, and molybdenum-oxygen-chloride complexes in the presence of reduced sulfur species (S^{2-}). Potash feldspathization, associated with Mo mineralization, consumed alkali ions and increased fluid pH. Following reaction illustrates molybdenite precipitation (Taner et al., 1998):

$$3KAlSi_3O_8 \; (K-feldspar+2H^++2H_2MoO_4+4H_2S)$$
$$= KAl_2(AlSi_3O_{10})(OH)_2 \; (sericite)$$
$$+ 2K^+ + 6SiO_2 + 2MoS_2 + 6H_2O + O_2$$

This reaction promote molybdenite precipitation, elevates ore forming fluid pH, and facilitates dissociation of the molybdenum-oxygen-chloride complex, enabling Mo deposition (Ulrich and Mavrogenes, 2008).

5.4 Ore genesis

The metal mineralization in the Binnan Mo deposit is spatially, temporally, and genetically associated with the Mesozoic granite pluton (Qi et al., 2017). The Re-Os isochron age of 142.9 ± 5.1 Ma to 143.7 ± 0.8 Ma obtained from molybdenite, aligns with the published age of granite formation (Figure 8; Qi et al., 2017). During Cretaceous, the westward subduction of the Paleo-Pacific Plate (Wang et al., 2013) and the closure of the Mongol-Okhotsk Ocean (Ouyang et al., 2015) initiated an extensional geodynamic setting, leading to the partial melting of a juvenile mafic lower crust. Geochemical data from the Mesozoic granite and ore samples of the Binnan Mo deposit suggest that multiple magmatic activities provided substantial heat sources for mineralization (Shu and Chiaradia, 2021). Large-scale intrusive magmatism supplied the necessary thermal energy for ore formation (Qi et al., 2017; Shu and Chiaradia, 2021). Substantial crust and mantle-derived materials, after partial melting, formed metal-enriched magma, which subsequently ascended along structural fracture zones, resulting in the separation of Mo-rich hydrothermal fluids. Mo-bearing ore-forming fluids were transported by the ascending magma, as evidenced by the H-O and S isotopes of quartz, molybdenite, and pyrite (Figures 7, 9; Shu et al., 2013). As the temperature of the ore-bearing hydrothermal fluids decreased, the solubility of molybdenum sulfides was reduced, leading to disseminated Mo mineralization. The influx of meteoric water further decreased the temperature and salinity of the mixed hydrothermal fluids, altering the thermodynamic and physicochemical conditions of the fluid system. Between 250°C and 320°C, the mixing of different fluids and metal concentration had the most significant impact on the precipitation of ore minerals, substantially decreasing the solubility of molybdenum sulfides and leading to the formation of hydrothermal Mo deposits. At 160°C–180°C, the appearance of polymetallic sulfides (predominantly pyrite) and carbonate minerals in large quantities marked the conclusion of the ore-forming process, ultimately resulting in the hydrothermal Mo deposits within rock mass fracture zones and the contact zones of dykes.

6 Conclusion

The main conclusions of this study are as follows:

(1) The molybdenite Re-Os dating indicates that the Binnan Mo deposit was formed during the late Jurassic, approximately 142.9 ± 5.1 Ma to 143.7 ± 0.8 Ma.

(2) 2. The mineralization process of the Binnan Mo deposit is characterized by three stages: the K-feldspar-quartz stage (I),

TABLE 2 Molybdenite Re-Os isotope data in the Binnan Mo deposit.

| No.	Re	Os	^{187}Re	^{187}Os	Age
ZK10402	56.94 ± 0.49	0.2870 ± 0.0599	35.79 ± 0.31	85.62 ± 0.54	143.4 ± 2.1
ZK10303	66.60 ± 0.52	0.1840 ± 0.0783	41.86 ± 0.32	100.3 ± 0.7	143.7 ± 2.0
ZK10004	51.84 ± 0.39	0.2251 ± 0.0459	32.58 ± 0.24	78.28 ± 0.54	144.0 ± 2.0
ZK10003	55.33 ± 0.56	0.1705 ± 0.0428	34.78 ± 0.35	83.39 ± 0.58	143.7 ± 2.3
ZK10404	56.94 ± 0.43	0.2456 ± 0.0641	35.79 ± 0.27	85.76 ± 0.50	143.7 ± 2.0
ZK2404	75.44 ± 0.67	0.2717 ± 0.0694	47.42 ± 0.42	113.6 ± 0.7	143.6 ± 2.1
ZK10405	58.80 ± 0.50	0.2439 ± 0.0647	36.96 ± 0.32	88.56 ± 0.51	143.7 ± 2.1
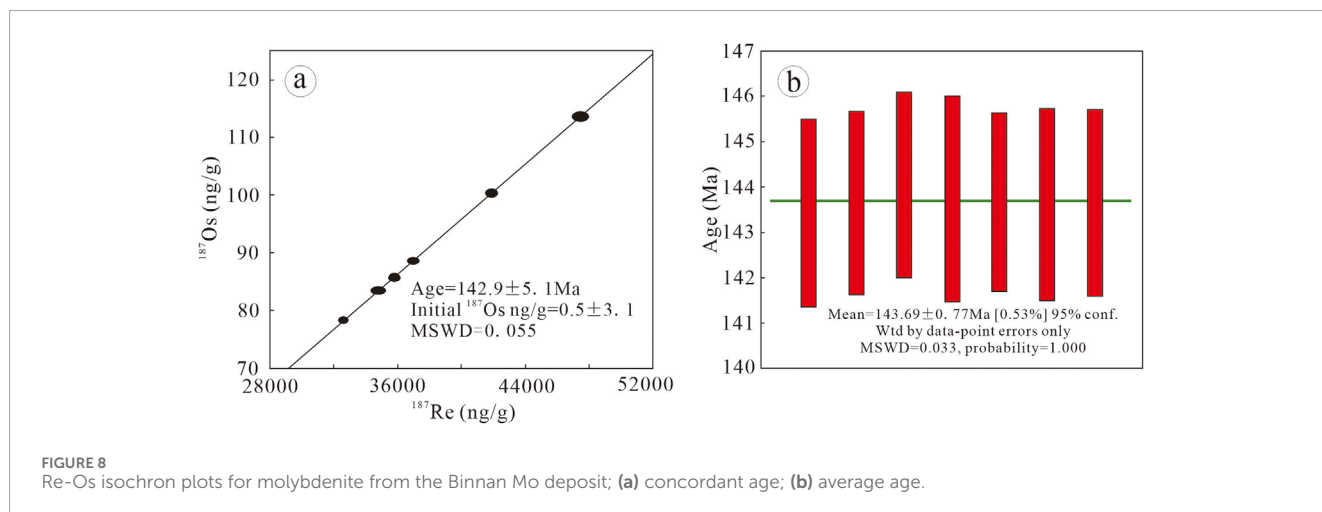
FIGURE 8
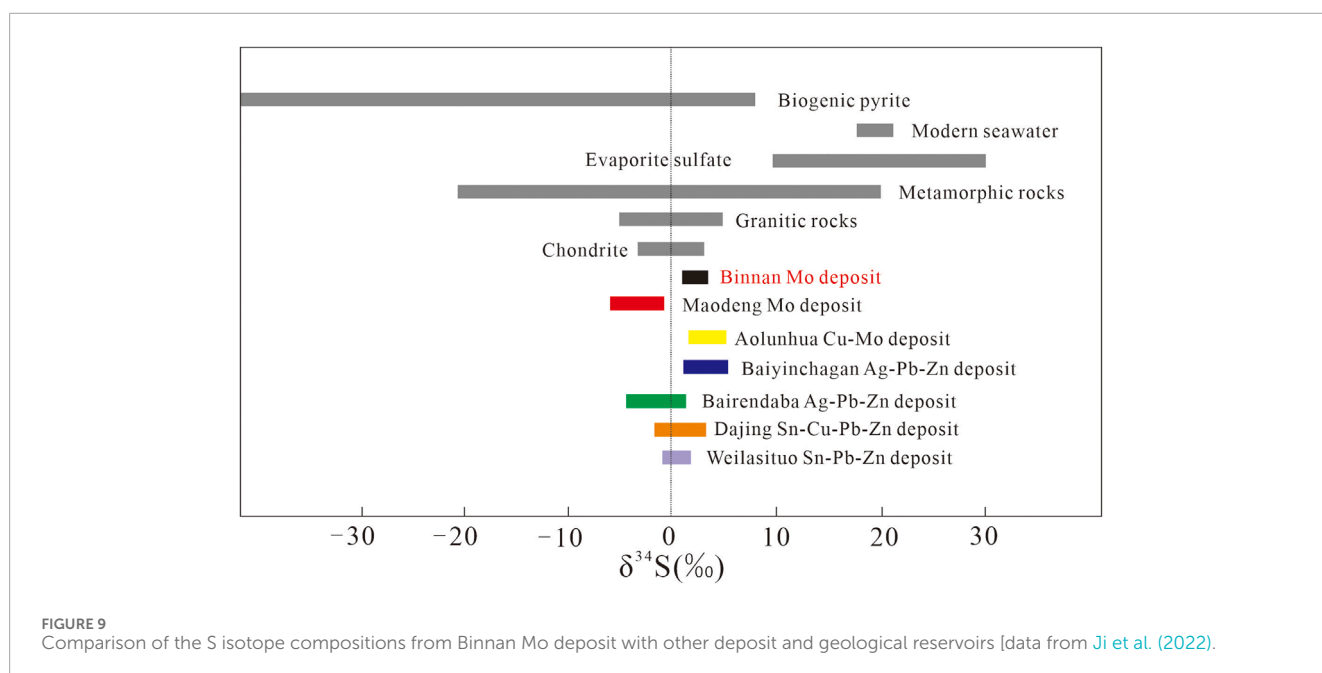Re-Os isochron plots for molybdenite from the Binnan Mo deposit; (a) concordant age; (b) average age.

FIGURE 9
Comparison of the S isotope compositions from Binnan Mo deposit with other deposit and geological reservoirs [data from Ji et al. (2022).

the quartz-molybdenite stage (II), and the quartz-calcite stage (III). Molybdenum precipitation predominantly occurred during stages I and II, with stage II being the most significant stage for Mo mineralization.

(3) The S isotopic values of molybdenite and pyrite from the Binnan Mo deposit range from 1.2‰ to 4.5‰ with an average of 2.69‰, indicating a magmatic source for sulfur in the ore-forming fluid.

(4) The H-O isotopic compositions of the Binnan Mo deposit (δD = −75.5‰ to −92.3‰; $\delta^{18}O$ = 13.3‰–15‰) suggest that the ore-forming fluids were magmatic in origin, gradually mixing with meteoric water during fluid evolution.

(5) Fluid mixing and temperature variations were the primary factors contributing to Mo deposition in the Binnan Mo deposit.

Data availability statement

The original contributions presented in the study are included in the article/supplementary material, further inquiries can be directed to the corresponding author.

Author contributions

ZQ: Writing–original draft. ST: Writing–review and editing. GuS: Writing–review and editing. GaS: Formal Analysis, Writing–review and editing. AM: Investigation, Writing–review and editing. XL: Methodology, Writing–review and editing. BD: Data curation, Writing–review and editing.

Funding

Conflict of interest

The authors declare that the research was conducted in the absence of any commercial or financial relationships that could be construed as a potential conflict of interest.

Generative AI statement

The author(s) declare that no Generative AI was used in the creation of this manuscript.

Publisher's note

All claims expressed in this article are solely those of the authors and do not necessarily represent those of their affiliated organizations, or those of the publisher, the editors and the reviewers. Any product that may be evaluated in this article, or claim that may be made by its manufacturer, is not guaranteed or endorsed by the publisher.

References

Chen, G. Z., Wu, G., Wu, W. H., Zhang, T., Li, T. G., Liu, R. L., et al. (2018). Fluid inclusion study and isotope characteristics of the Daolundaba copper-polymetallic deposit in the southern Great Xing'an Range. *Earth Sci. Front.* 25 (5), 202–221. (In Chinese with English abstract). doi:10.13745/j.esf.sf.2018.4.10

Chu, X. L., Hou, W. G., and Zhang, X. (2002). S, C and Pb isotopes and sources of metallogenetic elements of the Dajing Cu-polymetallic deposit in Linxi County, Inner Mongolia, China. *Acta Petrol. Sin.* 8 (4), 566–574. (In Chinese with English abstract).

Cox, S. F., Knackstedt, M. A., and Braun, J. (2001). Principles of structural control on permeability and fluid hydrothermal system. *Soc. Explor. Geophys. Rev.* 14, 1–24. doi:10.5382/Rev.14.01

Du, B. F., Wei, J. H., Wang, Q., Li, Y. J., Liu, G. C., Yu, H. T., et al. (2010). Discussion on metallogenic setting and time difference between magmatism and mineralization of molybdenum deposits in East China. *Mineral. Deposits* 29 (6), 935–955. (In Chinese with English abstract).

Glesemann, A., Jaeger, H. J., Norman, A. L., Krouse, H. R., and Brand, W. A. (1994). Online sulfur-isotope determination using an elemental analyzer coupled to a mass spectrometer. *Anal. Chem.* 66, 2816–2819. doi:10.1021/ac00090a005

Hao, Y. J., Ren, Y. S., Duan, M. X., Tong, K. Y., Chen, C., and Li, C. (2014). Re–Os isotopic dating of the molybdenite from the tongshan porphyry Cu–Mo deposit in Heilongjiang province, NE China. *Acta Geol. Sin.* 88 (s2), 522–523. (In Chinese with English abstract). doi:10.1111/1755-6724.12374_14

Hu, X., Yao, S., Ding, Z., and He, M. C. (2017). Early Paleozoic magmatism and metallogeny in Northeast China: a record from the Tongshan porphyry Cu deposit. *Min. Deposita* 52, 85–103. doi:10.1007/s00126-016-0653-0

Jahn, B., Windley, B., Natal'In, B., and Dobretsov, N. (2004). Phanerozoic continental growth in Central Asia. *J. Asian Earth Sci.* 23 (5), 599–603.

Ji, G. Y., Jiang, S. H., Liu, Y. F., Zhang, L. S., and Li, Q. L. (2022). Geology, molybdenite Re-Os age, H-O-S-Pb isotopes, and fluid inclusion features of the Maodeng Mo-Bi-Sn-Cu deposit, Inner Mongolia. *Ore Geol. Rev.* 150, 105157. doi:10.1016/j.oregeorev.2022.105157

Kudrin, A. V. (1989). Behavior of Mo in aqueous NaCl and KCl solutions at 300-450°C. *Geochem. Int.* 26 (8), 87–99.

Liu, J., Mao, J. W., Wu, G., Wang, F., Luo, D. F., Hu, Y. Q., et al. (2014). Fluid inclusions and H–O–S–Pb isotope systematics of the Chalukou giant porphyry Mo deposit, Heilongjiang Province, China. *Ore Geol. Rev.* 59, 83–96. doi:10.1016/j.oregeorev.2013.12.006

Liu, J., Wu, G., Li, Y., Zhu, M. T., and Wei, Z. (2012). Re–Os sulfide (chalcopyrite, pyrite and molybdenite) systematics and fluid inclusion study of the Duobaoshan porphyry Cu (Mo) deposit, Heilongjiang Province, China. *J. Asian Earth Sci.* 49 (3), 300–312. doi:10.1016/j.jseaes.2011.10.014

Long, X. Y., Tang, J., Xu, W. L., Sun, C. Y., Luan, J. P., and Guo, P. (2022). A crustal growth model for the eastern central asian orogenic belt: constraints from granitoids in the songnen Massif and duobaoshan terrane. *Gondwana Res.* 107, 325–338. doi:10.1016/j.gr.2022.04.001

Ma, X. H., and Chen, B. (2011). The source of hydrothermal fluids and mineralization in the Aolunhua porphyry Mo-Cu deposit, Southern Da Hinggan Mountains: constraints from stable (C, H, O and S) and radiogenic (Pb) isotopes. *J. Jilin Univ. Earth Sci. Ed.* 41 (6), 1770–1783. (In Chinese with English abstract).

Ohmoto, H., and Rye, R. O. (1979). "Isotope of sulfur and carbon," in *Geochemistry of hydrothermal ore deposit*. Editor H. L. Barnes 2nd ed. (New York: John Wiley and Sons), 509–567.

Ouyang, H. G., Mao, J. W., Zhou, Z. H., and Su, H. M. (2015). Late Mesozoic metallogeny and intracontinental magmatism, southern Great Xing'an Range, northeastern China. *Gondwana Res.* 27 (3), 1153–1172. (In Chinese with English abstract). doi:10.1016/j.gr.2014.08.010

Qi, Z. Y., Wang, S. P., Yang, Q. Q., Wang, Q., Gao, L. K., Chen, C., et al. (2017). Research on petrogeochemistry of host granodiorite in binnan

Mo deposit in da hinggan mountain. 37(4), 27–37. (In Chinese with English abstract).

Sheppard, S. M. F. (1986). Characterization and isotopic variations in natural waters. *Rev. Mineralogy Geochem.* 16 (1), 165–183.

Shu, Q., Chang, Z., Lai, Y., Hu, X., Wu, H., Zhang, Y., et al. (2019). Zircon trace elements and magma fertility: insights from porphyry (-skarn) Mo deposits in NE China. *Mineral. Deposits* 54, 645–656. doi:10.1007/s00126-019-00867-7

Shu, Q., and Chiaradia, M. (2021). Mesozoic Mo mineralization in northeastern China did not require regional-scale pre-enrichment. *Econ. Geol.* 116 (5), 1227–1237. doi:10.5382/econgeo.4823

Shu, Q., Lai, Y., Sun, Y., Wang, C., and Meng, S. (2013). Ore genesis and hydrothermal evolution of the Baiyinnuo'er zinc-lead skarn deposit, Northeast China: evidence from isotopes (S, Pb) and fluid inclusions. *Econ. Geol.* 108 (4), 835–860. doi:10.2113/econgeo.108.4.835

Shu, Q. H., Chang, Z. S., Lai, Y., Zhou, Y., Sun, Y., and Yan, C. (2016). Regional metallogeny of Mo-bearing deposits in northeastern China, with new Re-Os dates of porphyry Mo deposits in the northern Xilamulun district. *Econ. Geol.* 111 (7), 1783–1798. doi:10.2113/econgeo.111.7.1783

Taner, H., William, J. A. E., and Wood, S. A. (1998). The nature, origin and physicochemical controls of hydrothermal Mo-Bi mineralization in the Cadillac deposit, Quebec, Canada. *Miner. Deposita* 33 (6), 579–590. doi:10.1007/s001260050174

Ulrich, T., and Mavrogenes, J. (2008). An experimental study of the solubility of molybdenum in H2O and KCl-H2O solutions from 500°C to 800°C, and 150 to 300MPa. *Geochimica Cosmochimica Acta* 72 (9), 2316–2330. doi:10.1016/j.gca.2008.02.014

Wang, L. B., Ji, K. J., and Chen, D. (1997). Re-Os isotope ages of molybdenite from the Anjishan copper deposit and the Tongshan Cu-Mo deposit and their

implications. *Acta Petrologica Mineralogica* 16 (2), 154–159. (In Chinese with English abstract).

Wang, Y., Zhou, L. Y., and Zhao, L. J. (2013). Cratonic reactivation and orogeny: an example from the northern margin of the North China Craton. *Gondwana Res.* 24, 1203–1222. doi:10.1016/j.gr.2013.02.011

Yuan, M. W., Li, L., Li, S. R., Santosh, M., Li, C. L., Alam, M., et al. (2023). Direct radiometric dating of bitumen using Sm-Nd isotopes. *AAPG Bull.* 107 (11), 1883–1900. doi:10.1306/07062322106

Yuan, M. W., Li, L., Li, S. R., Santosh, M., Li, C. L., Masroor, A., et al. (2019). Mineralogy, fluid inclusions and S-Pb-H-O isotopes of the Erdaokan Ag-Pb-Zn deposit, Duobaoshan metallogenic belt, NE China: implications for ore genesis. *Ore Geol. Rev.* 113, 103074. doi:10.1016/j.oregeorev.2019.103074

Yuan, M. W., Li, S. R., Li, C. L., Santosh, M., Masroor, A., and Zeng, Y. J. (2018). Geochemical and isotopic composition of auriferous pyrite from the Yongxin gold deposit, Central Asian Orogenic Belt: implication for ore genesis. *Ore Geol. Rev.* 93, 255–267. doi:10.1016/j.oregeorev.2018.01.002

Yuan, M. W., Zeng, Y. J., Li, C. L., Li, S. S., and Li, S. R. (2017). Quantitative and positioning study on the hydrothermal alteration and mineralization relationship of the Yongxin gold deposit in the Nenjiang-Heihe mélange zone, Heilongjiang province. *Geoscience* 31 (2), 278–289.

Zhang, X. Z., Yang, B. J., Wu, F. Y., and Liu, G. X. (2006). The lithosphere structure in the Hingmong-Jihei (Hinggan-Mongolia-Jilin-Heilongjiang) region, northeastern China. *Geol. China* 33 (4), 816–823. (In Chinese with English abstract).

Zheng, Y. F., Fu, B., and Zhang, X. H. (1996). Effects of magma degassing on the carbon and sulfur isotope compositions of igneous rocks. *Sci. Geol. Sin.* 31 (1), 43–53. (In Chinese with English abstract).